Dalton Transactions

ROYAL SOCIETY OF CHEMISTRY

PAPER

View Article Online
View Journal | View Issue

Cite this: *Dalton Trans.*, 2020, **49**, 11648

Synthesis, dynamics and redox properties of eight-coordinate zirconium catecholate complexes†

Thomas H. Do and Seth N. Brown *

Received 15th July 2020,
Accepted 4th August 2020

DOI: 10.1039/d0dt02487b

rsc.li/dalton

Reaction of the 9,9-dimethylxanthene-bis(imine)-bis(catechol) ligand $XbicH_4$ with half an equivalent of Zr(acac)$_4$ affords the neutral tetracatecholate complex $(XbicH_2)_2Zr$, containing four iminium ions hydrogen bonded to the catecholates. The heteroleptic bis(catecholate)-tetraphenylporphyrin complex (TPP)Zr($XbicH_2$) is formed from reaction of (TPP)Zr(OAc)$_2$ with $XbicH_4$ in the presence of base. Both compounds adopt an eight-coordinate square antiprismatic geometry around the zirconium center. NMR spectra of (TPP)Zr($XbicH_2$) show that it is fluxional at room temperature, with homoleptic $(XbicH_2)_2Zr$ showing fluxionality at higher temperatures. Calculations and kinetic isotope effect measurements suggest that the motions involve dissociation of a single catecholate oxygen and subsequent twisting of the seven-coordinate species. The compounds show reversible one-electron oxidations of each of the bound catecholates to bound semiquinones.

Introduction

Catecholate ligands are famous for their ability to bind to metallic elements in the p, d, and f blocks and to adopt different oxidation states.[1] With oxophilic early d block elements such as titanium and zirconium, catecholates are excellent ligands, but their small size tends to favor oligomeric species or anionic compounds such as $[Ti(cat)_3]^{2-}$.[2] The poor ligating ability of oxidized catecholates, especially their propensity to dissociate as benzoquinones upon oxidation, has resulted in an absence of semiquinone complexes of group 4 metals. This contrasts with the existence of stable iminosemiquinone[3–5] and diiminosemiquinone complexes,[6,7] some of which are capable of effecting oxidative transformations of coordinated ancillary ligands.[8]

Recently, we reported the synthesis of a novel bis(iminocatecholate) ligand, $XbicH_4$, in which two electron-rich and sterically protected di-*tert*-butylcatecholate moieties are bridged by a 4,5-diamino-9,9-dimethylxanthene bridge.[9] The geometry of the xanthene bridge allows the catecholates to bind in a square array that is unusual for poly(catecholate) ligands. Additionally, the imine nitrogens can abstract a proton from the catecholate, allowing each catecholate to bind as an overall monoanion and thus accommodating polycatecholate complexes without large accompanying negative charges. Here we describe the preparation and characterization of very stable neutral eight-coordinate zirconium poly(catecholate) complexes containing one or two $XbicH_2^{2-}$ ligands.

Experimental

General procedures

Unless otherwise noted, all procedures were carried out in a drybox under an atmosphere of dry nitrogen. Dried solvents were purchased from Acros Organics and stored in the drybox. Deuterated solvents were purchased from Cambridge Isotope Laboratories. CD_2Cl_2 and $CDCl_3$ were dried over 4 Å molecular sieves, followed by CaH_2; C_6D_6 and $C_6D_5CD_3$ were dried over sodium; and tetrahydrofuran-d_8 was dried over sodium benzophenone ketyl. After being vacuum transferred from their drying agents, deuterated solvents were stored in the drybox. (TPP)Zr(OAc)$_2$ (H_2TPP = *meso*-tetraphenylporphyrin) was prepared according to literature procedures.[10] All other reagents were commercially available and used as received.

NMR spectra were measured on a Bruker Avance DPX 400 MHz or 500 MHz spectrometer. Chemical shifts for ^{1}H and $^{13}C\{^1H\}$ spectra are reported in ppm downfield of TMS, with spectra referenced using the known chemical shifts of the solvent residuals. Variable-temperature NMR spectra were taken on the Bruker Avance DPX 400 with temperatures calibrated using methanol or ethylene glycol standards.[11] Infrared spectra were recorded by ATR on a Jasco 6300 FT-IR spectrometer and are reported in wavenumbers. UV-visible spectra

Department of Chemistry and Biochemistry, University of Notre Dame, 251 Nieuwland Science Hall, Notre Dame, IN 46556-5670, USA.
E-mail: Seth.N.Brown.114@nd.edu

† Electronic supplementary information (ESI) available: Additional spectroscopic and electrochemical data and computational information. CCDC 2015704 and 2015705. For ESI and crystallographic data in CIF or other electronic format see DOI: 10.1039/d0dt02487b

were recorded in 1 cm quartz cells on a ThermoFisher Evolution Array diode array spectrophotometer or Jasco V-670 spectrophotometer. Elemental analyses were performed by M–H–W Laboratories (Phoenix, AZ, USA).

Syntheses

$(XbicH_2)_2Zr$. In the air, $XbicH_4$ (494.5 mg, 0.701 mmol) is dissolved in 10 mL of $CHCl_3$ and added to a 20 mL vial containing $Zr(acac)_4$ (160.8 mg, 0.330 mmol). The resulting blue solution is stirred for 12 h and filtered to remove any unreacted $Zr(acac)_4$. The solvent is removed *in vacuo* and the blue solid is collected and washed with 3 × 10 mL of 90/10 pentane/$CHCl_3$ to yield 436.2 mg $(XbicH_2)_2Zr$ (87%). ^{1}H NMR (CD_2Cl_2): δ 16.61 (d, 10 Hz, 2H, CH═N*H*), 15.01 (d, 11 Hz, 2H, CH═N*H*), 8.94 (d, 10 Hz, 2H, C*H*═NH), 8.87 (d, 11 Hz, 2H, C*H*═NH), 7.49 (m, 2H, 3-H), 7.39 (d, 7 Hz, 2H, 6-H), 7.34 (m, 4H, 1,2-H), 7.14 (t, 7 Hz, 2H, 7-H), 6.98 (d, 7 Hz, 2H, 8-H), 6.39 (s, 2H, cat ArH), 6.35 (s, 2H, cat ArH), 1.79 (s, 6H, C[C*H*$_3$][CH′$_3$]), 1.71 (s, 6H, C[CH$_3$][C*H*′$_3$]), 1.41 (s, 18H, ^{t}Bu), 1.37 (s, 18H, ^{t}Bu), 1.11 (s, 18H, ^{t}Bu), 0.94 (s, 18H, ^{t}Bu). ^{13}C{^{1}H} NMR (C_6D_6): δ 177.29 (H*C*═NH), 175.25 (H*C*═NH), 159.89, 159.08, 158.10, 157.53, 142.27, 141.87, 136.31, 136.15, 132.80, 132.25, 132.22, 130.46, 130.30, 129.93, 125.12, 124.99, 124.42, 123.78, 120.39, 120.12, 115.45, 115.38, 111.01, 110.25, 35.31, 35.25, 35.22, 35.11, 34.76, 33.75, 33.68 (C[*C*H$_3$]$_3$), 33.37 (C[*C*H$_3$]$_3$), 32.46, 29.36 (C[*C*H$_3$]$_3$), 29.26 (C[*C*H$_3$]$_3$). IR (cm^{-1}): 2968 (m), 2951 (m), 2911 (m), 2869 (m), 2851 (5), 1737 (w), 1727 (w), 1611 (s), 1596 (s), 1585 (s), 1513 (m), 1480 (s), 1449 (s), 1425 (m), 1394 (m), 1388 (m), 1373 (m), 1361 (m), 1344 (s), 1300 (m), 1278 (m), 1243 (s), 1211 (s), 1197 (m), 1171 (m), 1153 (m), 1110 (w), 1074 (w), 1028 (m), 993 (m), 985 (m), 978 (m), 876 (m), 861 (m), 832 (m), 820 (m), 799 (m), 780 (m), 738 (s), 699 (w), 689 (w), 669 (w), 662 (w). UV-vis (CH_2Cl_2): λ_{max} 270 nm (ε = 14 500 L mol^{-1} cm^{-1}), 370 (10 300), 568 (11 000). Anal. calcd for $C_{90}H_{108}N_4O_{10}Zr$: C, 72.21; H, 7.27; N, 3.74. Found: C, 72.46; H, 7.51; N, 3.49.

(TPP)Zr(XbicH$_2$). A solution of $XbicH_4$ (303.5 mg, 0.431 mmol) in 10 mL of $CHCl_3$ is added to a 20 mL vial containing (TPP)Zr(OAc)$_2$ (327.6 mg, 0.391 mmol) and K_2CO_3 (216.4 mg, 1.566 mmol). The reaction mixture is stirred for 10 h and suction filtered through a glass frit in the air to remove excess K_2CO_3. The solvent is removed *in vacuo* and the blue solid is collected and washed repeatedly with 3 mL portions of pentane until the blue color of the filtrate becomes pale (5–10 portions). Air-drying affords 469.0 mg (TPP)Zr(XbicH$_2$) (85%). ^{1}H NMR (THF-d_8, −58 °C): δ 11.30 (d, 12.5 Hz, 2H, HC═N*H*), 9.25 (s, 2H, pyrrole), 8.81 (d, 7.4 Hz, 2H, *o*-Ph), 8.64 (s, 2H, pyrrole), 8.37 (d, 12.6 Hz, 2H, *H*C═NH), 8.22 (d, 4.4 Hz, 2H, pyrrole), 8.13 (d, 7.4 Hz, 2H, *o*-Ph), 8.10 (d, 4.4 Hz, 2H, pyrrole), 7.91 (t, 7 Hz, 2H, *m*- or *p*-Ph), 7.89 (d, 7 Hz, 2H, *o*-Ph), 7.82 (t, 7.4 Hz, 2H), 7.80 (d, 7.1 Hz, 2H, *o*-Ph), 7.75 (t, 7.4 Hz, 2H, *m*- or *p*-Ph), 7.68 (t, 7.4 Hz, 2H, *m*- or *p*-Ph), 7.62 (t, 7.5 Hz, 2H, *m*- or *p*-Ph), 7.58 (d, 7.8 Hz, 2H, xanthene 3,6-H), 7.52 (t, 7.4 Hz, 2H, *m*- or *p*-Ph), 7.12 (t, 7.6 Hz, 2H, xanthene 2,7-H), 6.95 (d, 7.6 Hz, 2H, xanthene 1,8-H), 5.97 (s, 2H, cat ArH), 1.98 (s, 3H, C[C*H*$_3$][CH′$_3$]), 1.63 (s, 3H, C[CH$_3$][C*H*′$_3$]), 1.23 (s, 18H, ^{t}Bu), 0.66 (s, 18H, ^{t}Bu). ^{13}C{^{1}H} NMR ($CDCl_3$, −58 °C): δ 174.35 (H*C*═NH), 156.49, 154.42, 153.13, 150.65, 151.26, 150.65, 150.20, 143.23, 142.80, 139.74, 138.04, 137.70, 137.15, 135.58, 133.65, 131.88, 131.00, 129.14, 129.01, 128.60, 127.27, 126.95, 126.77, 126.71, 126.66, 126.48, 126.21, 125.65, 125.18, 123.85, 123.42, 120.53, 115.72, 106.65, 34.75, 34.58, 33.08 (C[*C*H$_3$]$_3$), 31.81, 30.08 (C[*C*H$_3$]$_3$), 22.88, 14.53. IR (cm^{-1}): 3077 (w), 3051 (w), 3023 (w), 2952 (m), 2900 (m), 2866 (m), 1615 (s), 1596 (s), 1583 (s), 1516 (m), 1478 (s), 1441 (m), 1425 (m), 1394 (m), 1375 (m), 1365 (m), 1341 (s), 1300 (m), 1283 (m), 1246 (s), 1228 (m), 1212 (m), 1197 (m), 1173 (m), 1155 (m), 1110 (m), 1072 (w), 1028 (w), 1000 (m), 984 (s), 925 (w), 919 (w), 878, (m), 868, (m), 831 (m), 823 (m), 798 (s), 779 (m), 753 (s), 736 (s), 721 (s), 702 (s), 687 (m), 670 (m), 659 (m). UV-vis (CH_2Cl_2): λ_{max} 384 nm (ε = 65 400 L mol^{-1} cm^{-1}), 431 (169 000), 558 (18 500) 592 (sh, 6850). Anal. calcd for $C_{89}H_{82}N_6O_5Zr$: C, 75.98; H, 5.88; N, 5.97. Found: C, 76.12; H, 5.68; N, 6.06. (TPP)Zr(XbicD$_2$) is made by dissolving a sample of (TPP)Zr(XbicH$_2$) in 50/50 MeOH-d_4/THF-d_8 in a sealed NMR tube. After 3 d, the solvent is evaporated and the sample dissolved in THF-d_8. NMR analysis shows that the sample is 95% deuterated.

Electrochemistry

Cyclic voltammograms were performed at a scan rate of 60 mV s^{-1} using a Metrohm Autolab PGSTAT128N potentiostat, with glassy carbon working and counter electrodes and a silver/silver chloride pseudo-reference electrode. The electrodes were connected to the potentiostat through electrical conduits in the drybox wall. Samples were 1 mM in analyte dissolved in CH_2Cl_2 with 0.1 M Bu_4NPF_6 as the electrolyte. Potentials were referenced to ferrocene/ferrocenium at 0 V.[12] The reference potentials were established by spiking each test solution with a small amount of decamethylferrocene (E° = −0.565 V *vs.* Cp_2Fe^+/Cp_2Fe).[13]

Redox titrations

In the drybox, in a 20 mL scintillation vial, approximately 0.015 g of the analyte was dissolved in 10 mL dichloromethane. An aliquot of this solution (of a volume appropriate for the intensity of the band being observed) was added to a septum-capped cuvette containing 2 mL dichloromethane. A stock solution of ferrocenium hexafluorophosphate, acetylferrocenium hexafluorophosphate,[14] or silver hexafluorophosphate was prepared by adding 0.005 g (0.015 g for more concentrated solutions) of the redox agent to a 20 mL scintillation vial and dissolving in 10 mL dichloromethane. An aliquot of this solution was transferred to a 2 mL vial and sealed with a septum cap and brought to the UV-Vis-NIR spectrophotometer.

The spectrophotometer was blanked against neat dichloromethane, and an initial spectrum of the neutral analyte was taken. Incremental additions of 5 μL of the redox agent solution were then syringed into the cuvette with an air-tight Hamilton syringe, and spectra were measured after each addition. The redox titration was deemed complete once no changes to the optical spectra were observed for five consecutive additions of redox agent.

X-ray crystallography

Crystals of $(XbicH_2)_2Zr{\cdot}3\ CHCl_3{\cdot}C_6H_{14}$ were grown from a solution of $(XbicH_2)_2Zr$ in $CHCl_3$ layered with hexanes. Crystals of $(TPP)Zr(XbicH_2){\cdot}7$ THF were grown from a solution of the compound in THF at room temperature. Crystals were placed in inert oil before being transferred to the cold N_2 stream of a Bruker Kappa X8-Apex-II or a Bruker Apex II CCD diffractometer, respectively. The data were reduced, correcting for absorption, using the program SADABS. The structures were solved using direct methods. All nonhydrogen atoms were refined anisotropically. In $(TPP)Zr(XbicH_2){\cdot}7$ THF, hydrogen atoms were found on difference maps and refined isotropically except for those on the lattice THF. In $(XbicH_2)_2Zr{\cdot}3\ CHCl_3{\cdot}C_6H_{14}$, only the hydrogens on the imine carbon and nitrogen atoms were found and refined. All other hydrogens were placed in calculated positions with their thermal parameters tied to the isotropic thermal parameters of the atoms they are bonded (1.5× for methyl, 1.2× for all others).

In $(XbicH_2)_2Zr{\cdot}3\ CHCl_3{\cdot}C_6H_{14}$, one chloroform of solvation in the asymmetric unit was found and refined, but there was additional diffuse electron density in the unit cell that was treated using the program SQUEEZE.[15] The total amount of electron density found in the void spaces was 421 electrons per unit cell, corresponding to approximately four $CHCl_3$ and four hexane molecules per unit cell. Disorder was noted in C13S of one of the THF solvate molecules in $(TPP)Zr(XbicH_2){\cdot}7$ THF. The disorder was modeled by refining the disordered atom in two sites with a total occupancy of unity, fixing the thermal parameters of the two sites to be equal and allowing their relative occupancies to refine. Calculations used SHELXTL (Bruker AXS),[16] with scattering factors and anomalous dispersion terms taken from the literature.[17] Further details are in Table 1.

Variable-temperature NMR spectroscopy

Variable-temperature ^1H NMR spectra of $(TPP)Zr(XbicH_2)$ and $(TPP)Zr(XbicD_2)$ were acquired in THF-d_8 from −72 °C to 55 °C and of $(XbicH_2)_2Zr$ in 1,2-dichlorobenzene-d_4 from 23 °C to 135 °C. Lineshapes were simulated using iNMR.[18] For $(TPP)Zr(XbicH_2)$ and its deuterated analogue, the pyrrole proton resonances were simulated, while for $Zr(XbicH_2)_2$, the *tert*-butyl resonances were simulated. For temperatures above the coalescence point, chemical shifts were estimated by linear extrapolation of the temperature-dependent shifts, and the extrapolated differences in chemical shift were treated as fixed in the simulation, with a constant (small) offset added to all chemical shifts if needed to align with the observed average shift.

Computational methods

Geometry optimizations were performed on $(XbicH_2)_2Zr$ and $(TPP)Zr(XbicH_2)$ using density functional theory (B3LYP, SDD basis set for Zr, 6-31G* for other atoms) as implemented in the Gaussian16 suite of programs.[19] The X-ray structures were used as initial geometries, with all *tert*-butyl, methyl, and phenyl groups replaced by hydrogen. The optimized geometries of ground state species were confirmed as minima, and those of transition states as first-order saddle points, by calculation of vibrational frequencies. Plots of calculated Kohn–Sham orbitals were generated using Gaussview (v. 6.0.16) with an isovalue of 0.04.

Table 1 Crystal data for $(XbicH_2)_2Zr{\cdot}3\ CHCl_3{\cdot}C_6H_{14}$ and $(TPP)Zr(XbicH_2){\cdot}7$ THF

	$(XbicH_2)_2Zr{\cdot}3\ CHCl_3{\cdot}C_6H_{14}$	$(TPP)Zr(XbicH_2){\cdot}7$ THF
Molecular formula	$C_{99}H_{125}Cl_9N_4O_{10}Zr$	$C_{117}H_{138}N_6O_{12}Zr$
Formula weight	1941.37	1911.55
T/K	120(2)	120(2)
Crystal system	Monoclinic	Monoclinic
Space group	$C2/c$	$P2_1/n$
λ/Å	0.71073 (Mo Kα)	0.71073 (Mo Kα)
Total data collected	99 143	326 985
No. of indep reflns.	12 983	24 610
R_{int}	0.0308	0.0655
Obsd refls [$I > 2\sigma(I)$]	11 050	19 848
a/Å	35.0034(17)	20.745(3)
b/Å	12.2378(7)	17.732(2)
c/Å	24.6829(12)	28.218(4)
α/°	90	90
β/°	133.9561(12)	108.6014(18)
γ/°	90	90
V/Å^3	9477.3(8)	9838(2)
Z	4	4
μ/mm^{-1}	0.341	0.179
Crystal size/mm	0.34 × 0.26 × 0.26	0.41 × 0.21 × 0.19
No. refined params	528	1563
R_1, wR_2 [$I > 2\sigma(I)$]	0.0406, 0.1077	0.0469, 0.1024
R_1, wR_2 [all data]	0.0504, 0.1151	0.0639, 0.1093
Goodness of fit	1.051	1.041

Results and discussion

Metalation of $XbicH_4$ to form eight-coordinate zirconium catecholate complexes

The bis(catechol) ligand $XbicH_4$ reacts with various zirconium(IV) starting materials, such as $Zr(NEt_2)_4$, $Zr(CH_2Ph)_4$, or $Zr(acac)_4$, to give the eight-coordinate complex $(XbicH_2)_2Zr$ (eqn (1)). The resulting blue compound is air- and water-stable, with spectra taken after a month of exposure to air as a solid or in solution indicating no discernible degradation of the complex. Even in the presence of an excess of zirconium, only the homoleptic complex is formed from the amide or alkyl starting materials, but an intermediate mixed-ligand complex $(XbicH_2)Zr(acac)_2$ forms in reactions with a 1 : 1 ratio of $XbicH_4$ and $Zr(acac)_2$ (Fig. S3†).

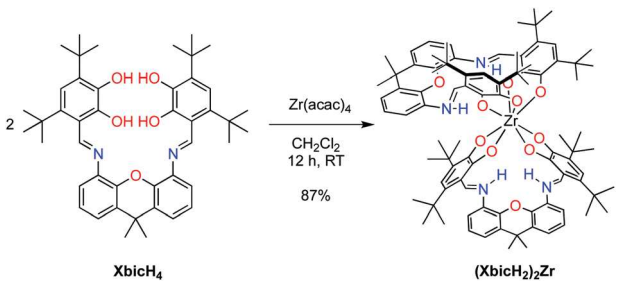

(1)

NMR spectra of $(XbicH_2)_2Zr$ indicate that the compound has C_2 symmetry with the twofold axis passing between the

ligands, giving rise to a single, but unsymmetrical, $XbicH_2$ environment. This is inconsistent with a dodecahedral (D_{2d}-symmetric) environment in which the two ligand planes are perpendicular, as is seen in previously prepared zirconium complexes with bis(catecholate) ligands.[20,21] The large coupling constants (10–11 Hz) in the ^{1}H NMR spectra between the two downfield signals at 16.61 and 15.01 ppm and the two imine C*H* peaks at δ 8.94 and 8.87 indicate that the ligands have adopted an iminium–catecholate structure, a motif well known in metal complexes of mono-deprotonated catecholimines.[9,22–26]

To prepare a heteroleptic $XbicH_2$ complex, the tetraphenylporphyrin complex $(TPP)Zr(OAc)_2$[10] is used as a starting material. Treatment of this reagent with $XbicH_4$ in the presence of base yields the desired product, $(TPP)Zr(XbicH_2)$ (eqn (2)). This eight-coordinate complex is slightly air- and water sensitive, undergoing about 10% decomposition to an unknown product after a week exposed to air in CD_2Cl_2.

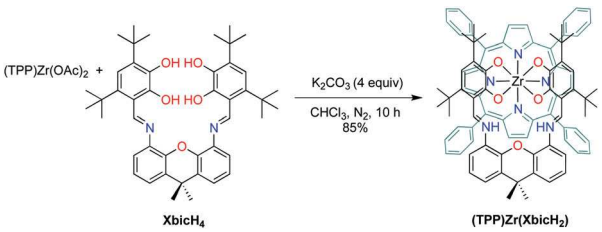

(2)

Spectroscopic features of $(TPP)Zr(XbicH_2)$ are consistent with molecular C_s symmetry, with the presence of two pyrrole singlets and two pyrrole doublets (^3J = 4.5 Hz) in the ^{1}H NMR indicating that the mirror plane bisects two of the pyrrole rings (rather than passing through the *meso* carbons of the porphyrin). The 12 Hz coupling between the *H*C═N*H* protons confirms that protons are bound to the $XbicH_2$ imine nitrogens.

Structures of zirconium catecholate complexes

The solid-state structure of $(XbicH_2)_2Zr$ (Fig. 1) displays the C_2 symmetry implied by the solution NMR spectra, with the midlines of the ligands (as measured by the Zr–O5 vector) rotated by 143°. Zirconium adopts a square antiprismatic coordination geometry, with the four catecholate oxygens from one $XbicH_2$ ligand forming each of the square faces. In previously characterized tetracatecholate complexes of group 4 metals, both square antiprismatic[27] and dodecahedral[20,21,28] geometries have been observed, so the geometry of $Zr(XbicH_2)_2$ is likely due to the preference of the Xbic ligand to occupy a roughly square coordination array, as shown in its silicon complexes.[9] The larger Zr atom is much farther out of the O_4 plane than is silicon (1.20 Å *vs.* 0.47 Å); this is accommodated by twisting about the xanthene–nitrogen bonds (dihedral angles of roughly 32°), which allows the zirconium to remain roughly in the plane of the catecholates.

The solid state structure of $(TPP)Zr(XbicH_2)_2$ (Fig. 2) shows a very similar Zr–$XbicH_2$ coordination geometry, with the (non-crystallographic) mirror plane through the $XbicH_2$ ligand

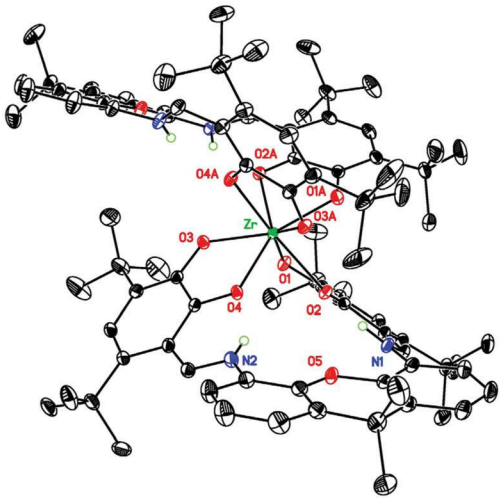

Fig. 1 Thermal ellipsoid plot of $(XbicH_2)_2Zr{\cdot}3\ CHCl_3{\cdot}C_6H_{14}$. Lattice solvent molecules and hydrogen atoms bonded to carbon have been omitted for clarity.

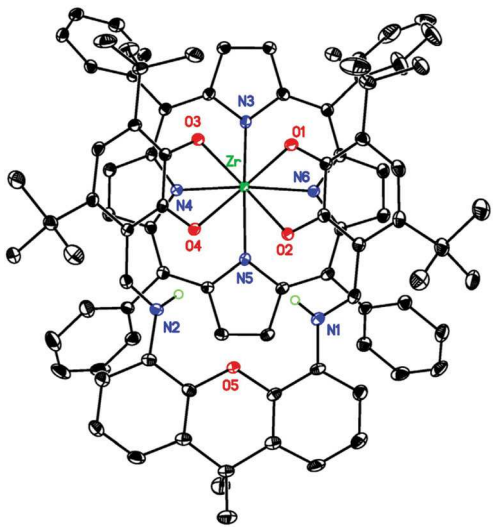

Fig. 2 Thermal ellipsoid plot of the cation of $(TPP)Zr(XbicH_2){\cdot}7$ THF. Lattice solvent molecules and hydrogen atoms bonded to carbon have been omitted for clarity.

coinciding with a mirror plane that bisects the pyrrole rings in the porphyrin, consistent with the NMR data for this compound. Again, zirconium adopts a square antiprismatic geometry, which is unsurprising since all eight-coordinate zirconium porphyrin compounds adopt this geometry.[10,29–33] The zirconium is equidistant from the two ligands (1.217 Å from the O_4 plane and 1.214 Å from the N_4 plane).

In each $XbicH_2$ ligand, the two remaining acidic hydrogens are found on difference maps and are clearly bonded to the nitrogen atoms. Inspection of the bond lengths in the ligand indicates that there are characteristic bond length changes that suggest that the enaminoketone resonance structure is

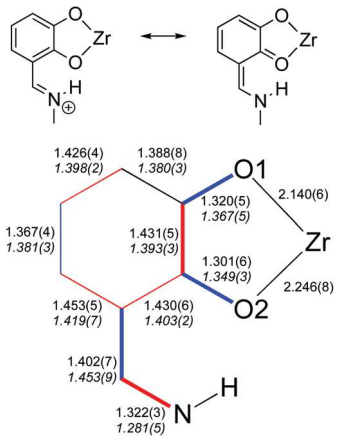

Fig. 3 Structural comparison between Zr(XbicH$_2$) complexes (avg. bond lengths in Roman type) and free XbicH$_4$ (ref. 9, avg. bond lengths in *italics*). The bonds shown in red are significantly longer in the Zr complexes, while the bonds in blue are significantly shorter.

more significant in the zirconium complexes than, for example, in the parent ligand XbicH$_4$ (Fig. 3), which adopts a catechol–imine structure.[9] The bond lengths are close to those shown by organic compounds that adopt the NH tautomer in the solid state,[34] for which both the neutral and zwitterionic resonance structures are significant contributors.[35] Both the greater ketone character of O2 and its strong hydrogen bond to the NH group make O2 a weaker donor than O1, and the Zr–O2 bond length is consistently about 0.10 Å longer than Zr–O1 (Table 2).

Dynamics of ligand twisting in (XbicH$_2$)Zr complexes

At low temperature (<−30 °C in THF-d_8), the ^{1}H NMR spectrum of (TPP)Zr(XbicH$_2$) is consistent with the C_s symmetry exhibited by the compound in the solid state (Fig. 4). In particular,

Table 2 Selected metrical data for (XbicH$_2$)$_2$Zr·3 CHCl$_3$·C$_6$H$_{14}$ and (TPP)Zr(XbicH$_2$)·7 THF

	(XbicH$_2$)$_2$Zr·3 CHCl$_3$·C$_6$H$_{14}$	(TPP)Zr(XbicH$_2$)·7 THF[a]
Bond distances/Å		
Zr–O1	2.1459(12)	2.135(4)
Zr–O2	2.1446(11)	2.249(6)
Zr–O3	2.2489(11)	—
Zr–O4	2.2359(11)	—
Zr–N3	—	2.3335(15)
Zr–N4	—	2.380(4)
Zr–N5	—	2.3631(15)
Bond angles/°		
O1–Zr–O3	77.93(5)	75.84(5)
O1–Zr–O2	70.19(4)	70.4(4)
O1–Zr–O2A	78.83(4)	—
O1–Zr–N3	—	79(3)
N3–Zr–N4	—	75.00(15)

[a] Where applicable, chemically equivalent parameters in the crystal structure have been averaged between values related by the (noncrystallographic) mirror planes through the center of the molecules. The cited esd's combine the variance of the independent values with the esd's of each individual observation.

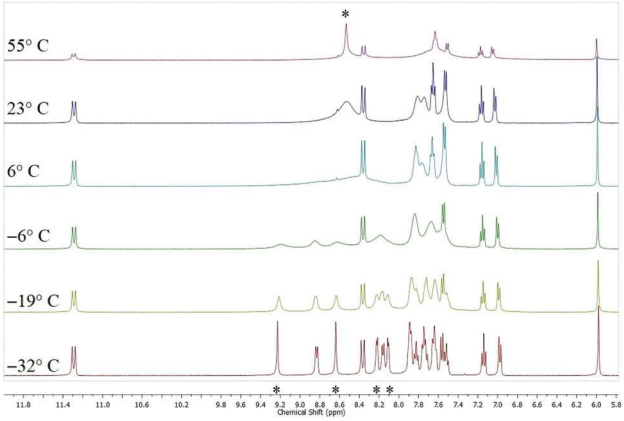

Fig. 4 Variable-temperature ^{1}H NMR (aromatic region) for (TPP)Zr(XbicH$_2$) (THF-d_8, 400 MHz). Pyrrole peaks are marked with *.

the tetraphenylporphyrin ligand exhibits four inequivalent pyrrole resonances and ten peaks for the *meso* phenyl groups. As the temperature is raised, all the TPP resonances broaden. While the lineshapes of the *ortho* and *meta* protons of the phenyl rings are complicated by hindered phenyl group rotation,[36–39] the broadening and coalescence of the four pyrrole resonances are characteristic of a net rotation of the XbicH$_2$ mirror plane relative to the porphyrin, resulting in a change in the time-averaged symmetry of the porphyrin from C_s to C_{4v}. The XbicH$_2$ signals remain sharp and unshifted, indicating that the molecule maintains the same overall structure at all temperatures.

The homoleptic complex (XbicH$_2$)$_2$Zr also shows dynamic behavior by ^{1}H NMR spectroscopy (Fig. 5), albeit with an onset at a much higher temperature (100 °C *vs.* −20 °C for (TPP)Zr(XbicH$_2$)). As the temperature is raised, the resonances related by reflection in the plane bisecting each XbicH$_2$ ligand exchange, though the geminal methyl groups on the dimethylxanthene remain sharp and inequivalent even at the highest temperatures that could be achieved. Activation parameters for

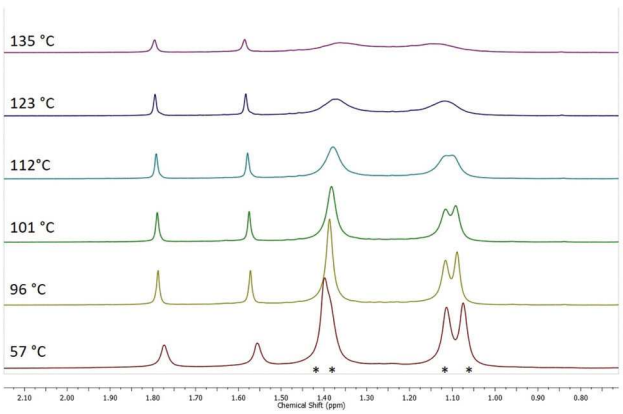

Fig. 5 Variable-temperature ^{1}H NMR (aliphatic region) for (XbicH$_2$)$_2$Zr (1,2-dichlorobenzene-d_4, 400 MHz). Exchanging *tert*-butyl groups are marked with *.

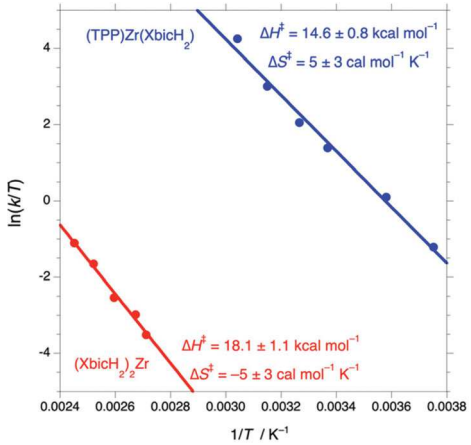

Fig. 6 Eyring plots for relative twisting of the tetradentate ligands for (TPP)Zr($XbicH_2$) (blue) and for Zr($XbicH_2$)$_2$ (red).

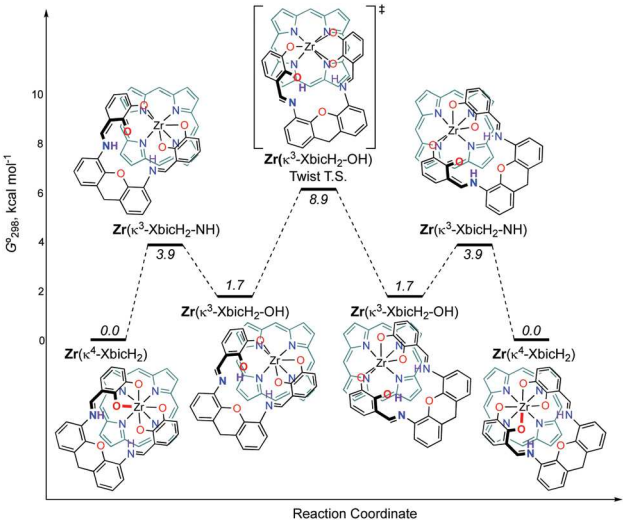

Fig. 7 Calculated energy landscape (B3LYP, SDD/6-31G*) for net ligand rotation in (Por)Zr($XbicH_2$). The ligand fragment that dissociates from the zirconium over the course of the reaction is highlighted in bold.

the fluxional processes in both compounds are ascertained from Eyring plots of rate constants determined by lineshape simulation (Fig. 6).

The mechanisms of the net twisting of the two tetradentate ligands relative to each other have been clarified through DFT calculations. In zirconium bis(porphyrin) complexes, such a tetragonal twist appears to be so difficult as to be experimentally unobservable. Both zirconium octaalkyl[40] and tetraarylporphyrins[39] are stereochemically rigid by ^{1}H NMR at temperatures up to 150 °C. Rotamers of bis(porphyrin)zirconium do not interconvert even at 110 °C over the course of 2 h,[36,39] giving a barrier to twisting of >32 kcal mol^{-1}. This agrees with the results of DFT calculations on (porphine)$_2$Zr, for which the D_{4h} transition state to twisting is found to have $\Delta G^{\ddagger}$ = 32.6 kcal mol^{-1} (Table 3).

The monoporphyrin complex (Por)Zr($XbicH_2$) is computed to be only marginally more stable as an 8-coordinate species than it is as a seven-coordinate complex with one $XbicH_2$ oxygen dissociated (**Zr**(κ^3-$XbicH_2$–NH) in Fig. 7). Once dissociated, the enaminoketone form with an NH group is about 2 kcal mol^{-1} less stable than its iminophenol tautomer with an OH group (**Zr**(κ^3-$XbicH_2$–OH)), as expected based on the iminophenol structure found in free $XbicH_4$.[9] In the seven-coordinate structure, rotation of the tridentate ligand with respect to the tetradentate porphyrin is rapid (through the Twist T.S., $\Delta G^{\ddagger}$ = 7.2 kcal mol^{-1} for the OH tautomer, 7.1 kcal mol^{-1} for the NH tautomer). This agrees with the high fluxionality of seven-coordinate Zr porphyrins reported in the literature. For example, the 8-coordinate porphyrin dimer ((TPP)Zr)$_2$(μ-S$_2$)$_2$ shows a static ^{1}H NMR spectrum at room temperature, while seven-coordinate [((TPP)Zr)$_2$(μ-OH)$_3$]$^+$ and ((TPP)Zr)$_2$(μ-O)(μ-OH)$_2$ are fluxional even at −50 °C.[31]

Since the barriers to rotation in the NH and OH tautomers are essentially the same, the reaction is expected to proceed through the more stable OH tautomer, if proton transfer is reasonably facile. Computationally, the calculated barrier to proton transfer in the seven-coordinate intermediate is 5.1 kcal mol^{-1} lower than the overall rotation barrier, consistent with a fast pre-equilibrium among tautomers. Experimentally, the dynamics of the deuterated compound (TPP)Zr($XbicD_2$) are observed to be identical to its protio analogue (k_H/k_D = 1.02 ± 0.06, Fig. S4, S5 and Table S1†), ruling out rate-limiting proton transfer (which would have a primary kinetic isotope effect). The small secondary kinetic isotope effect due to the stronger hydrogen bonding in the dissociated ligand (calculated k_H/k_D = 1.13) is consistent with the insensitivity of the NMR dynamics to deuteration.

The homoleptic ($XbicH_2$)$_2$Zr has a similar calculated energy landscape (Fig. S6†), though with a significantly higher overall barrier to rotation of 14.8 kcal mol^{-1}. The trends in computed barrier are thus in good agreement with the experimentally observed trends of (Por)$_2$Zr ≫ ($XbicH_2$)$_2$Zr > (Por)Zr($XbicH_2$), though the DFT calculations appear to systematically underestimate the magnitudes of the barriers. The major factor in lowering the barrier to rotation of the $XbicH_2$ complexes appears to be its greater ability (compared to porphyrin) to partially dissociate to form a highly fluxional seven-coordinate

Table 3 Experimental and calculated (B3LYP, 6-31G*/SDD) activation barriers for relative twisting of the tetradentate ligands in 8-coordinate zirconium complexes. Free energies of activation are at 298 K unless otherwise noted. Por = TPP for experimental data, porphine for calculated barriers unless otherwise noted

Compound	$\Delta G^{\ddagger}_{expt}$, kcal mol^{-1}	$\Delta G^{\ddagger}_{DFT}$, kcal mol^{-1}
(Por)$_2$Zr	>32[a]	32.6
(Por)Zr($XbicH_2$)	13.11(5)	8.9
($XbicH_2$)$_2$Zr	19.6(2)	14.8[b]
		16.0[c]

[a] Por = 5,15-di-*p*-tolylporphyrin, ref. 36; Por = TPP-NO_2, ref. 39. [b] *Via* a 7-coordinate transition state. [c] *Via* an 8-coordinate transition state.

complex. This is consistent with the observation that while bis(porphyrin)zirconium complexes are stereochemically rigid, dynamics are observed in the presence of Brønsted acids,[36] which might stabilize a seven-coordinate intermediate by protonating the porphyrin. It should be noted that, in contrast to (Por)Zr(XbicH$_2$), an eight-coordinate (cubic) transition state could be found computationally for (XbicH$_2$)$_2$Zr (Fig. S6†) at only slightly higher energies than the seven-coordinate transition state, leaving open the possibility that the homoleptic complex might undergo ligand rotation without partial ligand dissociation.

Optical spectroscopy, electrochemistry and bonding of (XbicH$_2$)Zr complexes

The optical spectrum of (XbicH$_2$)$_2$Zr (Fig. 8) shows a very broad, moderate-intensity transition centered at 568 nm and a much more intense transition in the near-UV at 369 nm. With the aid of time-dependent DFT calculations, the lower-energy band is assigned to excitations from the catecholate redox-active orbitals (RAOs, consisting of the in-phase combination of oxygen pπ orbitals that is antibonding with respect to the benzene π orbitals[41]) to a ligand orbital that is principally C═N π* in character. A red shift of this transition (observed at 343 nm in free XbicH$_4$)[9] upon complexation has been previously observed in a dioxomolybdenum(VI) complex of an allyliminium–catecholate ligand, which absorbs at about 450 nm.[25] The much lower energy of the transition in the zirconium complex is likely due to the electropositive Zr rendering the catecholate more electron-rich and hence raising the energy of the HOMO. The higher-energy band in (XbicH$_2$)$_2$Zr is assigned to excitations from the other catecholate oxygen π orbitals (out of phase, bonding with respect to the benzene π orbitals) to the C═N π* orbitals.

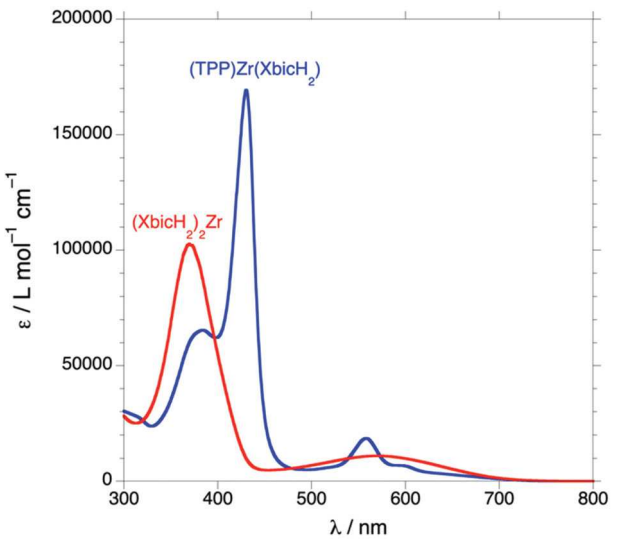

Fig. 8 UV-visible spectra (CH_2Cl_2) of (XbicH$_2$)$_2$Zr (red trace) and (TPP)Zr(XbicH$_2$) (blue trace).

In the mixed-ligand (TPP)Zr(XbicH$_2$), similar bands can be seen superimposed on the familiar Q-band (λ_{max} = 558, 592 nm) and Soret band (430 nm) due to the porphyrin. The porphyrin absorptions are red-shifted by ~20 nm relative to the bands in (TPP)Zr(OAc)$_2$ (Fig. S7†).

Cyclic voltammetry of (XbicH$_2$)$_2$Zr and (TPP)Zr(XbicH$_2$) shows well-separated, reversible one-electron oxidation waves for each of the catecholate groups (Fig. 9 and Table 4). The porphyrin ligand in (TPP)Zr(XbicH$_2$) also shows oxidation (0.86 V and 1.12 V) and reduction (−1.99 V, −2.31 V) waves. The porphyrin-based oxidations are shifted to higher potential, and reductions to lower potential, compared to (TPP)Zr(OAc)$_2$ (Fig. S8†).

Further insight into the nature of the oxidized species is afforded by redox titration, monitored by UV-vis-NIR spectroscopy (Fig. 10 and S9†). One-electron oxidation of (TPP)Zr(XbicH$_2$) to [(TPP)Zr(XbicH$_2$)]$^+$ leads to the appearance of a feature of moderate intensity in the red (λ_{max} = 797 nm, ε = 1800 L mol^{-1} cm^{-1}). This feature is typical of semiquinone complexes of diamagnetic metals,[42] and is similar to features seen in group 4 iminosemiquinonate complexes,[4] consistent with oxidation taking place at the catecholate moiety. The porphyrin bands undergo small (~7 nm) hypsochromic shifts on oxidation, inconsistent with the gross changes in absorption typically associated with oxidation at the porphyrin ligand (*e.g.*, ~50 nm blue shifts on oxidation of Zr(OEP)$_2$ to [Zr(OEP)$_2$]$^+$).[43] A very broad feature in the near-IR (λ_{max} = 1200 nm) that grows in on one-electron oxidation is assigned

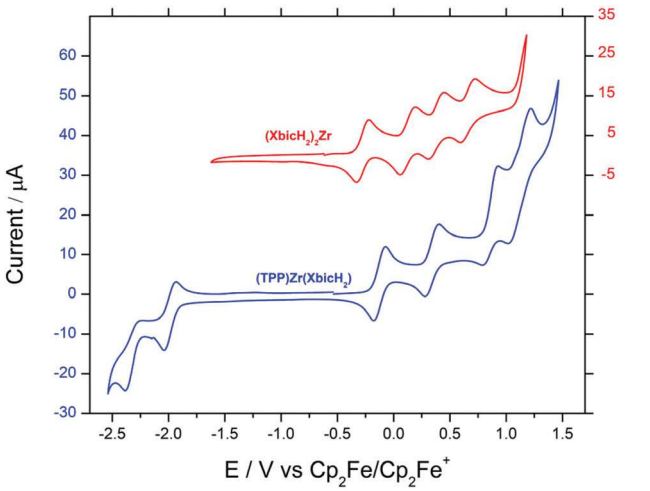

Fig. 9 Cyclic voltammograms (CH_2Cl_2, 60 mV s^{-1}, 0.1 M Bu$_4$NPF$_6$) of (XbicH$_2$)$_2$Zr (upper red trace) and (TPP)Zr(XbicH$_2$) (lower blue trace).

Table 4 Redox potentials (V *vs.* Cp$_2$Fe$^+$/Cp$_2$Fe, CH_2Cl_2, 0.1 M Bu$_4$NPF$_6$) for catecholate-based oxidations in (XbicH$_2$)$_2$Zr and (Por)Zr(XbicH$_2$)

Compound	Ox$_1$	Ox$_2$	Ox$_3$	Ox$_4$
(XbicH$_2$)$_2$Zr	−0.28	0.13	0.38	0.66
(Por)Zr(XbicH$_2$)	−0.13	0.34		

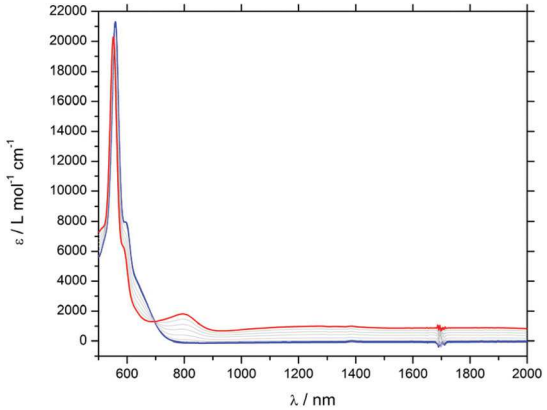

Fig. 10 Redox titration of (TPP)Zr(XbicH$_2$) (6×10^{-5} M, CH_2Cl_2) with $[Cp_2Fe]PF_6$. Initial spectrum is in blue, final spectrum is in red.

to an intervalence transition between the catecholate and semiquinone moieties of the Xbic ligand. This assignment is supported by the fact that removal of a second electron results in loss of this feature, while the semiquinone-based band shifts (to 819 nm) and increases in intensity (Fig. S9†). Similar changes in the long-wavelength region of the optical spectrum of $(XbicH_2)_2Zr$ are observed on one- and two-electron oxidation (Fig. S10†), except that the near-IR feature persists in $[(XbicH_2)_2Zr]^{2+}$. This is not surprising, since the doubly oxidized homoleptic compound still retains ligands in mixed oxidation states.

Consistent with the locus of oxidation being on the XbicH$_2$ groups, DFT calculations indicate that the HOMO of each complex is a combination of the catecholate redox-active orbitals (Fig. 11a and b). The homoleptic complex $(XbicH_2)_2Zr$ is calculated to have a set of four high-lying orbitals corresponding to the four possible RAO combinations, while the porphyrin has a similar set of four orbitals comprising the two RAO combinations as well as the nonbonding a_{2u} and a_{1u} orbitals[44] of the porphyrin. In a square antiprismatic coordination geometry, only the d_{z^2} orbital is not σ* in character, and weak π donation from the ligand RAOs to this orbital can be discerned in the HOMO−3 of each complex (Fig. 11c and d). However, the electrochemical data (for example, the relatively uniform separations of the four oxidations in $(XbicH_2)_2Zr$) suggest that this interaction has little energetic significance. This is consistent with the known weakness of π interactions between iminoxolene ligands and group 4 metals;[5] the dioxolene ligands' π donor orbitals are even lower in energy and would thus be expected to interact even more weakly with the high-energy d orbitals of an early transition metal like zirconium. The calculations on (Por)Zr(XbicH$_2$) indicate some mixing between the porphyrin a_{2u} orbital and the in-phase RAO combination, but again the electrochemistry, with its well-separated waves for catecholate and porphyrin oxidations, suggest that this mixing is not physically significant.

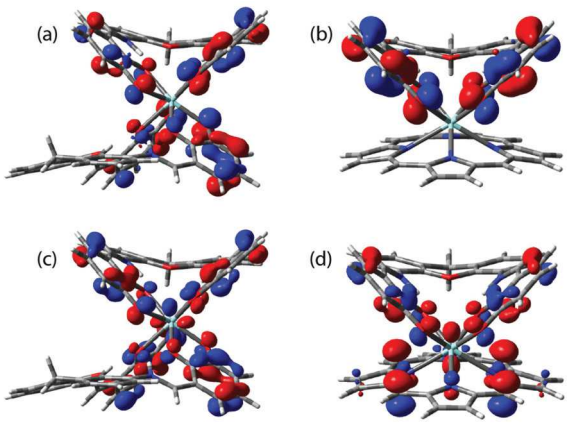

Fig. 11 Selected Kohn–Sham orbitals in $(XbicH_2)_2Zr$ (a, HOMO; c, HOMO−3) and (Por)Zr(XbicH$_2$) (b, HOMO; d, HOMO−3).

Conclusions

Eight-coordinate zirconium complexes of the bis(iminium-catecholate) ligand $XbicH_2^{2-}$ can be synthesized from a variety of ZrX_4 reagents (to form $(XbicH_2)_2Zr$) or with $(TPP)Zr(OAc)_2$ (to form (TPP)Zr(XbicH$_2$)). The complexes have square antiprismatic geometries, with each bis(catecholate) ligand spanning a square face. In contrast to stereochemically rigid bis(porphyrin)zirconium complexes, the XbicH$_2$ complexes display net twisting of the square faces of the antiprisms relative to each other by NMR, with the mixed-ligand complex showing the greater degree of fluxionality. The twisting most likely takes place because the XbicH$_2$ ligand is better able to adopt a κ^3 structure compared to the porphyrin. Electrochemical or chemical oxidation of the catecholate rings in the complexes takes place at moderate potentials to give spectroscopically observable semiquinone complexes.

Conflicts of interest

There are no conflicts to declare.

Acknowledgements

This work was supported by the US National Science Foundation (Grant CHE-1465104). We thank Dr Allen G. Oliver for his assistance with X-ray crystallography. T. H. D. acknowledges support from an Arthur J. Schmitt Fellowship.

Notes and references

1 C. G. Pierpont, *Coord. Chem. Rev.*, 2001, **216–217**, 99–125.
2 P. Zanello and M. Corsini, *Coord. Chem. Rev.*, 2006, **250**, 2000–2022.
3 K. J. Blackmore, J. W. Ziller and A. F. Heyduk, *Inorg. Chem.*, 2005, **44**, 5559–5561.

4 K. J. Blackmore, M. B. Sly, M. R. Haneline, J. W. Ziller and A. F. Heyduk, *Inorg. Chem.*, 2008, **47**, 10522–10532.
5 T. Marshall-Roth, K. Yao, J. A. Parkhill and S. N. Brown, *Dalton Trans.*, 2019, **48**, 1427–1435.
6 N. A. Ketterer, H. Fan, K. J. Blackmore, X. Yang, J. W. Ziller, M.-H. Baik and A. F. Heyduk, *J. Am. Chem. Soc.*, 2008, **130**, 4364–4374.
7 K. M. Clark, J. Bendix, A. F. Heyduk and J. W. Ziller, *Inorg. Chem.*, 2012, **51**, 7457–7459.
8 M. R. Haneline and A. F. Heyduk, *J. Am. Chem. Soc.*, 2006, **128**, 8410–8411.
9 T. H. Do and S. N. Brown, *Dalton Trans.*, 2019, **48**, 11565–11574.
10 J. L. Huhmann, J. Y. Corey, N. P. Rath and C. F. Campana, *J. Organomet. Chem.*, 1996, **513**, 17–26.
11 A. J. Gordon and R. A. Ford, *The Chemist's Companion*, John Wiley and Sons, New York, 1972.
12 N. G. Connelly and W. E. Geiger, *Chem. Rev.*, 1996, **96**, 877–910.
13 D. Lionetti, A. J. Medvecz, V. Ugrinova, M. Quiroz-Guzman, B. C. Noll and S. N. Brown, *Inorg. Chem.*, 2010, **49**, 4687–4697.
14 J. Jiao, G. J. Long, L. Rebbouh, F. Grandjean, A. M. Beatty and T. P. Fehlner, *J. Am. Chem. Soc.*, 2005, **127**, 17819–17831.
15 P. van der Sluis and A. L. Spek, *Acta Crystallogr., Sect. A: Found. Crystallogr.*, 1990, **46**, 194–201.
16 G. M. Sheldrick, *Acta Crystallogr., Sect. A: Found. Crystallogr.*, 2007, **64**, 112–122.
17 A. J. C. Wilson, *International Tables for Crystallography*, Kluwer Academic Publishers, Dordrecht, The Netherlands, 1992, vol. C.
18 iNMR (http://www.inmr.net).
19 M. J. Frisch, G. W. Trucks, H. B. Schlegel, G. E. Scuseria, M. A. Robb, J. R. Cheeseman, G. Scalmani, V. Barone, G. A. Petersson, H. Nakatsuji, X. Li, M. Caricato, A. V. Marenich, J. Bloino, B. G. Janesko, R. Gomperts, B. Mennucci, H. P. Hratchian, J. V. Ortiz, A. F. Izmaylov, J. L. Sonnenberg, D. Williams-Young, F. Ding, F. Lipparini, F. Egidi, J. Goings, B. Peng, A. Petrone, T. Henderson, D. Ranasinghe, V. G. Zakrzewski, J. Gao, N. Rega, G. Zheng, W. Liang, M. Hada, M. Ehara, K. Toyota, R. Fukuda, J. Hasegawa, M. Ishida, T. Nakajima, Y. Honda, O. Kitao, H. Nakai, T. Vreven, K. Throssell, J. A. Montgomery Jr., J. E. Peralta, F. Ogliaro, M. J. Bearpark, J. J. Heyd, E. N. Brothers, K. N. Kudin, V. N. Staroverov, T. A. Keith, R. Kobayashi, J. Normand, K. Raghavachari, A. P. Rendell, J. C. Burant, S. S. Iyengar, J. Tomasi, M. Cossi, J. M. Millam, M. Klene, C. Adamo, R. Cammi, J. W. Ochterski, R. L. Martin, K. Morokuma, O. Farkas, J. B. Foresman and D. J. Fox, *Gaussian 16, Revision B.01*, Gaussian, Inc., Wallingford CT, 2016.
20 S. Fritzsche, P. Lönnecke, T. Höcher and E. Hey-Hawkins, *Z. Anorg. Allg. Chem.*, 2006, **632**, 2256–2267.
21 S. H. Chikkali, D. Gudat, F. Lissner, M. Niemeyer, T. Schleid and M. Nieger, *Chem. – Eur. J.*, 2009, **15**, 482–491.
22 S. V. Baryshnikova, E. V. Bellan, A. I. Poddel'sky, M. V. Arsenyev, I. V. Smolyaninov, G. K. Fukin, A. V. Piskunov, N. T. Berberova, V. K. Cherkasov and G. A. Abakumov, *Eur. J. Inorg. Chem.*, 2016, **2016**, 5230–5241.
23 A. I. Poddel'sky, M. V. Arsen'ev, L. S. Okhlopkova, I. V. Smolyaninov and G. K. Fukin, *Russ. J. Coord. Chem.*, 2017, **43**, 843–851.
24 M. Albrecht, S. Burk, R. Stoffel, A. Lüchow, R. Fröhlich, M. Kogej and C. A. Schalley, *Eur. J. Inorg. Chem.*, 2007, 1361–1372.
25 H. A. Rudbari, M. Khorshidifard, B. Askari, N. Habibi and G. Bruno, *Polyhedron*, 2015, **100**, 180–191.
26 L. M. D. R. S. Martins, S. Hazra, M. F. C. Guedes da Silva and A. J. L. Pombeiro, *RSC Adv.*, 2016, **6**, 78225–78233.
27 C. J. Gramer and K. N. Raymond, *Inorg. Chem.*, 2004, **43**, 6397–6402.
28 (*a*) S. R. Sofen, S. R. Cooper and K. N. Raymond, *Inorg. Chem.*, 1979, **18**, 1611–1616; (*b*) G. E. Freeman and K. N. Raymond, *Inorg. Chem.*, 1985, **24**, 1410–1417.
29 K. Kim, W. S. Lee, H. J. Kim, S. H. Cho, G. S. Girolami, P. A. Gorlin and K. S. Suslick, *Inorg. Chem.*, 1991, **30**, 2652–2656.
30 J. L. Huhmann, J. Y. Corey and N. P. Rath, *Acta Crystallogr., Sect. C: Cryst. Struct. Commun.*, 1995, **51**, 195–196.
31 S. Ryu, D. Whang, H.-J. Kim, K. Kim, M. Yoshida, K. Hashimoto and K. Tatsumi, *Inorg. Chem.*, 1997, **36**, 4607–4609.
32 E. Stulz, H.-B. Bürgi and C. Leumann, *Chem. – Eur. J.*, 2000, **6**, 523–536.
33 A. Tutaß, M. Klöpfer, H. Hückstädt, U. Cornelissen and H. Homborg, *Z. Anorg. Allg. Chem.*, 2002, **628**, 1027–1044.
34 H. Pizzala, M. Carles, W. E. E. Stone and A. Thevand, *J. Chem. Soc., Perkin Trans. 2*, 2000, 935–939.
35 K. Ogawa, Y. Kasahara, Y. Ohtani and J. Harada, *J. Am. Chem. Soc.*, 1998, **120**, 7107–7108.
36 K. Tashiro, K. Konishi and T. Aida, *Angew. Chem., Int. Ed. Engl.*, 1997, **36**, 856–858.
37 M. Takeuchi, T. Imada, M. Ikeda and S. Shinkai, *Tetrahedron Lett.*, 1998, **39**, 7897–7900.
38 S. S. Eaton and G. R. Eaton, *J. Am. Chem. Soc.*, 1975, **97**, 3660–3666.
39 G. S. Girolami, P. A. Gorlin and K. S. Suslick, *Inorg. Chem.*, 1994, **33**, 626–627.
40 J. W. Buchler and G. Heinz, *Chem. Ber.*, 1996, **129**, 201–205.
41 D. J. Gordon and R. F. Fenske, *Inorg. Chem.*, 1982, **21**, 2907–2915.
42 C. W. Lange, B. J. Conklin and C. G. Pierpont, *Inorg. Chem.*, 1994, **33**, 1276–1283.
43 J. P. Collman, J. L. Kendall, J. L. Chen, T. A. Eberspacher and C. R. Moylan, *Inorg. Chem.*, 1997, **36**, 5603–5608.
44 M. O. Senge, A. A. Ryan, K. A. Letchford, S. A. MacGowan and T. Mielke, *Symmetry*, 2014, **6**, 781–843.